Chemogenomic screening Identifies the Hsp70 Co-chaperone HDJ2 as a Hub for Anticancer Drug Resistance

Nitika[1], Jacob S. Blackman[1], Laura E. Knighton[1], Jade E. Takakuwa[1], Stuart K. Calderwood[2] and Andrew W. Truman[1]*

[1]Department of Biological Sciences, University of North Carolina Charlotte, Charlotte, NC 28223, USA

[2]Department of Radiation Oncology, Beth Israel Deaconess Medical Center, Harvard Medical School, 330 Brookline Ave, Boston, MA 02215, USA

* Correspondence: atruman1@uncc.edu

Running title: HDJ2 regulates anticancer drug resistance

Keywords: Hsp70, HDJ2, molecular chaperones, chemogenomic screen, anticancer drug resistance.

The authors declare no potential conflicts of interest.

Abstract

Heat shock protein 70 (Hsp70) is an important molecular chaperone that regulates oncoprotein stability and tumorigenesis. However, attempts to develop anti-chaperone drugs targeting molecules such as Hsp70 have been hampered by toxicity issues. Hsp70 is regulated by a suite of co-chaperone molecules that bring “clients” to the primary chaperone for efficient folding. Therefore, rather than targeting Hsp70 itself, here we have examined the feasibility of inhibiting the co-chaperone HDJ2, a member of the J domain protein family, as a novel anticancer strategy. We found HDJ2 to be upregulated in a variety of cancers, suggesting a role in malignancy. To confirm this role, we screened the NIH Approved Oncology collection for chemical-genetic interactions with loss of HDJ2 in cancer. 41 compounds showed strong synergy with HDJ2 loss, whereas 18 dramatically lost potency. Several of these hits were validated using a HDJ2 inhibitor (116-9e) in castration-resistant prostate cancer cell (CRPC) and spheroid models. Taken together, these results confirmed that HDJ2 is a hub for anticancer drug resistance and that HDJ2 inhibition may be a potent strategy to sensitize cancer cells to current and future therapeutics.

Introduction

Hsp70 is a molecular chaperone that plays important roles in protein quality control processes such as protein folding, transport, degradation, regulation and aggregation prevention [1]. Hsp70 levels are elevated in various cancers and overexpression correlates with poor prognosis for survival and response to cancer therapy [2]. The elevated levels of Hsp90 and Hsp70 chaperones in cancer and their role in fostering multiple oncogenic pathways has made these proteins attractive drug targets with numerous anti-chaperone compounds having been developed so far [3]. Problematically, Hsp70 is required for cell survival and protein homeostasis, and thus its inhibition is detrimental to the viability of both normal and cancer cells, with dubious selectivity for tumor cells [4].

Hsp70 performs all its functions in association with a large spectrum of helper proteins known as co-chaperones that include J-proteins, tetratricopeptide repeat (TPR) domain-containing proteins and nucleotide exchange factors (NEFs) which fine-tune Hsp70 specificity and activity in the cell. The J-proteins recruit the protein substrates or clients and interact with such clients at the interface of NBD and SBDβ of Hsp70 [5]. This interaction leads to increased Hsp70-mediated ATP turnover and activation of protein folding. J-proteins have a highly conserved 70 amino acid motif containing Histidine, Proline and Aspartic acid amino acid residues known as HPD motif which is essential for stimulating ATPase activity of Hsp70 [6]. In humans, the J-protein family has about 50 members which are further divided into three groups based on the localization of J domain within a protein [7, 8]. DNAJA1 (more commonly referred to as HDJ2) associates with unfolded polypeptide chains, preventing their aggregation [7]. Several Hsp70 inhibitors

have failed in clinical trials due to their toxicity. More recently, alternative strategies have focused on sensitizing cells to anticancer agents by either manipulating post-translational modification of chaperones or their interaction with specific co-chaperones [4, 9-19]. HDJ2 (mammalian homologue of yeast Ydj1) is an interesting possible anticancer target as a key mediator of Hsp70 function that appears to regulate specific features of tumorigenesis [13, 20, 21]. A recent study demonstrated that CRPCs expressing ARv7 are insensitive to Hsp90 inhibitors but are sensitive to Hsp40 inhibition [22]. In addition, we have shown that targeting specific oncoprotein complexes (ribonucleotide reductase) with a combination of traditional as well as an HDJ2 inhibitor produces highly synergistic effects [13]. We propose that targeting HDJ2 in cancer may offer an attractive alternative to the toxicity induced by full Hsp90/Hsp70 inhibition.

Anticancer monotherapies using broadly active cytotoxic or molecularly targeted drugs are limited in their ability to demonstrate a reliable clinical response. This is due to redundant signaling pathways, feedback loops and resistance mechanisms in the cancer cells [23, 24]. Thus, combination anticancer therapies have been used clinically for over 50 years to improve the responses achieved by monotherapies alone. Cancer cell line-based models for these combination therapies are easy and inexpensive to perform using high-throughput drug screening protocols (HTS) to identify the most effective drug combination [25, 26]. HTS helps to explore the relation between the cell line characteristics and drug specific dose responses [25]. Chemogenomics is one such HTS based approach where large collection of anticancer chemical drugs are screened to identify biological targets. These screening sets often contain small molecules that are well annotated and have defined molecular targets. Such an approach is particularly

beneficial for cancer research because malignant cells often contain multiple aberrations which require targeted therapy to inactivate cancer driver activities and mitigate deleterious effects of the drugs to normal cells [24, 27].

Here, we performed an unbiased screen of the NIH Approved Oncology Drug set containing 131 anti-cancer drugs in combination with HAP1 cancer cell lines depleted of J-protein HDJ2. We identified 41 compounds showing strong synergy with the loss of HDJ2, and by contrast 18 molecules displaying reduced potency in the knockout cell line. We validated three drugs (cabozantinib, clofarabine and vinblastine) in combination with a unique HDJ2 inhibitor (116-9e) for synergy in the LNCaP cancer cell lines and confirmed omacetaxine mepesuccinate, idarubicin and sorafenib for antagonism (i.e. with reduced potency after HDJ2 inhibition). This study demonstrates the validity of developing Hsp70 co-chaperone inhibitors to sensitize cells to current anticancer therapies and suggests that determining HDJ2 status of a tumor may be beneficial in selecting the most appropriate course of treatment.

Materials and Methods

Cell culture. The HAP1 Chronic Myelogenous Leukemia cancer cell line and HDJ2 Knockout cell line was purchased from Horizon Discovery and were cultured in Iscove's Modified Eagle Medium (Invitrogen) with 10% fetal bovine serum (Gibco), 100 units/ml penicillin, and 100 µg/ml streptomycin at 5% CO_2 and 37° C. The LNCaP cancer cell line was purchased from ATCC and were cultured in RPMI-1640 medium (Invitrogen) with 10% fetal bovine serum (FBS, Clontech), 100 units/ml penicillin, and 100 µg/ml streptomycin at 5% CO_2 and 37° C.

Drug Screening. Approved Oncology Drug plates consisting of the most current FDA approved anticancer drugs were obtained from National Cancer Institute (NCI). For experiments delineating the synergy between the loss of HDJ2 and approved anticancer drug, HAP1 cells and HAP1 (HDJ2 KO) cells were plated in growth media at 20% confluency 1 day prior to drug treatment. On Day 1 of treatment, cells were treated with DMSO (control), Approved oncology anticancer drugs at 50 μM for 72 hours. Following drug treatments, Cell Titer-Glo reagent was added directly to the wells according to manufacturer's instructions. The luminescence was measured on Bio-Tek Plate reader. Luminescence reading was normalized to and expressed as a relative percentage of the plate averaged DMSO control. The data shown are the mean and SEM of three independent biological replicates.

Combination index (CI) calculations. For IC_{50} calculations, LNCaP cells were seeded in triplicates in 96-well white bottom Nunc plates in growth media at 20% confluency 1 day prior to initiation of drug treatment. On Day 1 of treatment, cells were treated with DMSO (control) and ten folds serial dilution of anti-cancer drugs Cabozantinib, Clofarabine, Vinblastine, Sorafenib, Idarubicin and Omacetaxine mepesuccinate and 116-9e. After 72 h, cell viability was measured using Promega Cell Titer-Glo cell viability assay on Bio-Tek plate reader. The combination index was calculated using the Chou-Talalay method using CompuSyn software[28].

Spheroid Generation. Single-cell suspensions (5000/well) were plated in one well of 24-well plates in a 1:1 mixture of RPMI medium and Matrigel (BD Bioscience CB-40324). Cells in Matrigel are kept cold at all times and under continuous agitation. Warm PBS is added to all empty wells, if any. Plates are incubated at 37 °C with 5% CO_2 for 15 min to

solidify the gel before addition of 100 µl of pre-warmed RPMI to each well. Two days after seeding, medium is fully removed and replaced with fresh RPMI containing the indicated drugs. The same procedure is repeated daily on two consecutive days. Twenty-four hours after the last treatments, media is removed and wells are washed with 100 µl of pre-warmed PBS. To prepare for downstream assays, spheroids are then released from Matrigel by incubating at 37 °C for 40 min in 100 µl of 10 mg/mL dispase (Sigma).

Apoptosis assay. Apoptosis of LNCaP spheroids was detected by the Annexin V–FITC/propidium iodide–binding assay. Cells were treated with either 0.1% DMSO (dimethyl sulfoxide),116-9e, Cabozantinib, Clofarabine, Vinblastine, Sorafenib, Idarubicin, Omacetaxine mepesuccinate and Sorafenib alone or in combination with 116-9e for 48 hours at the IC_{50} concentrations, and then stained with Annexin V–FITC and propidium iodide. The rate of apoptosis was determined using BD FORTESSA, and data were analyzed using FlowJo software and were reported as the mean ± SD. The results are representative of three independent experiments.

Bioinformatics. Cancer genome data and Cancer Cell Line Encyclopedia data were accessed from the cBioPortal (www.cbioportal.org) for Cancer Genomics (Gao et al, 2013). Total patient numbers and detailed information regarding published datasets and associated publications are indicated in Fig 1A and 1B.

Statistical analysis. Data were analyzed using GraphPad Prism built-in statistical tests indicated in relevant figure legends. The following asterisk system for P value was used: P <0.05; P <0.01; 0.001; and P <0.0001.

Results

HDJ2 is mutated and overexpressed in a variety of cancers.

We first investigated the incidence of HDJ2 alterations in cancer using cancer genomics databases. Mutations and copy number changes occur in HDJ2 at a relatively low level (<5% of samples) in the majority of cancer types (Figure 1). However, the data shows that HDJ2 is strikingly amplified in neuroendocrine prostate cancer (NEPC) at a frequency of 18.42% (Figure 1A). Additionally, HDJ2 is mutated in 11.1% of Non-Small Cell Lung Cancer (NSCLC) cases (Figure 1A). Hsp70 and Hsp90 are often overexpressed in tumors [2, 29, 30]. To determine if the HDJ2 gene is also overexpressed in cancer, we analyzed the expression data from 72,175 samples in 236 studies (cBioportal database) [31, 32]. Interestingly, HDJ2 was expressed at significantly higher levels in cancer samples, with a median expression in cancer of between log2 values of 10 and 14 (Figure 1B). Taken together, these data suggest that alteration of HDJ2 function may be important in the malignant properties of cancer cells.

Characterizing the role of HDJ2 in anticancer drug resistance.

The existing literature is contradictory as to whether HDJ2 may possess tumor suppressor or driver properties [21, 33].To clarify whether silencing of HDJ2 could be beneficial in the treatment of cancer, we screened wildtype HAP1 cells and HAP1 cells lacking HDJ2 ($HAP1^{HDJ2\ KO}$) for comparative resistance against the NIH NCI Approved Oncology Collection (Figure 2A) (https://dtp.cancer.gov/organization/dscb/obtaining/available_plates.html). According to pharmacologic action, the compounds in the library have been divided into seven categories: Protein synthesis inhibitors, Proteasome inhibitors, Epigenetic modifiers, Metabolic inhibitors, Cytoskeletal inhibitors, Signal transduction inhibitors and DNA

synthesis and repair inhibitors. Further fold enrichment of each drug category was calculated for the drugs whose potency increased or decreased with HDJ2 KO. To monitor the screening quality, each screening plate contained control wells treated with vehicle (1% DMSO). The final concentration of the screening compounds was 50 μmol/L. Positive hits (synergistic) or negative hits (antagonistic) were determined by normalizing the $\log_2$ ratio of viability of HDJ2 knockout cells over wildtype cells. A full list of the screening results is shown in Supplementary Table T1 and the sorted data are graphically plotted in Figure 2B. 41 drugs had increased potency upon HDJ2 deletion whereas 18 drugs displayed reduced potency. Drug target analysis was carried out by calculating fold enrichment of positive hits (synergistic) or negative hits (antagonistic) over the total number of drugs in that category. Drug target analysis of the synergistic drug hits revealed significant enrichment in DNA synthesis and repair inhibitors, epigenetic modifiers, signal transduction and cytoskeletal inhibitors (Figure 2C). In contrast, drug target analysis of antagonistic drug hits revealed a higher enrichment in categories such as epigenetic modifiers, protein synthesis inhibitors, cytoskeletal inhibitors and proteasome inhibitors (Figure 2D).

Strikingly, compounds from different categories showed dissimilar distribution of $\log_2$ ratio of viability, implying that different pharmacologic mechanisms probably underlie the HDJ2 inhibitory capacity. Category no. 6 (Signal Transduction inhibitors) contained the most hits which were synergistic with HDJ2 loss. Loss of HDJ2 also substantially increased the potency of DNA synthesis and repair (DDR) inhibitors. These results are in agreement with our previous study showing that HDJ2 plays an important role in maintaining the

stability of ribonucleotide reductase (RNR) complex which is important for DNA synthesis [13].

Validation of anticancer drugs significantly altered for potency upon loss of HDJ2. Many anticancer compounds have low potency, poor therapeutic index or suffer from development of resistance [34]. Monotherapy is rarely efficient and instead drug cocktails are widely used in the clinic [23, 26]. Establishing these combinations can enhance the scope of preclinical studies and inform the design of future clinical trials. Although several compounds were identified as becoming significantly more potent in cells lacking HDJ2, it remained to be determined whether small molecule inhibition of HDJ2 could produce a similar result. Our previous bioinformatics analysis indicated that a large proportion of prostate cancer cells contain either amplification or mutation of HDJ2 (approximately 18%, see Figure 1). Therefore, we next analyzed the effect of treating prostate cancer cells (LNCaP) with a combination of 116-9e, a small molecule inhibitor of HDJ2 [35] and interesting hits from our screen. We decided to focus on three synergistic drugs discovered in the screen: cabozantinib (receptor tyrosine kinase inhibitor), clofarabine (an RNR inhibitor) [36] and vinblastine (microtubule inhibitor/G2 arresting agent) [37-40]. We also validated three drugs that demonstrated a significant loss of potency in cells lacking HDJ2: sorafenib (a VEGFR-2 inhibitor) [41], omacetaxine mepesuccinate (more commonly known as homoharringtonine, a protein translation inhibitor) [42] and idarubicin (topoisomerase II inhibitor) [43].To determine synergy in a quantitative manner, we calculated drug synergy (Combination Index values, CI) between 116-9e and either synergistic or antagonistic drugs hits across a broad range of concentrations using the

Chou-Talalay method [44]. For three hits identified in our screen (cabozantinib, clofarabine and vinblastine) we confirmed significant synergy (CI<1) with 116-9e across a range of doses (Figure 3A, B & C). In contrast, idarubicin, omacetaxine and sorafenib displayed a significantly antagonistic interaction (CI>1) across a range of doses (Figure 3D, E & F).

These data suggest that while HDJ2 inhibition is a promising strategy to sensitize cells to some inhibitors, it might have inverse effects with other inhibitors.

Evaluating the effects of dual targeting of identified drugs with HDJ2 inhibition on morphology and viability of prostate cancer spheroids.

Recent studies have suggested that precision therapy approaches involving the exposure of drugs directly to the primary tumor tissue have the potential to augment the personalized medicine efforts and influence clinical decisions [45, 46]. Establishing *ex vivo* three-dimensional (3D) tumor spheroids or organoids derived from primary cancers can be easily established and potentially scaled to screen drug combinations [47]. These 3D cancer models appear to recapitulate features of the tumor of origin in terms of heterogeneity, cell differentiation, histoarchitecture, and clinical drug response and can be used for rapid drug screening [48]. We therefore next examined the effect of drug combination (three antagonistic and synergistic hits) on LNCaP spheroids. Specifically, changes in spheroid size and shape induced by the 3 antagonistic and synergistic drugs were determined. Visual examination revealed that for the synergistic drugs combination with 116-9e resulted in physical disruption of LNCaP spheroids, resulting in decrease in apparent spheroid size (Figure 4A). The disruption started on the second day of the

treatment. However, when the 3 antagonistic drugs were administered along with 116-9e, there were minimal changes in spheroid morphology indicating that the combination was ineffective.

Next, we measured the induction of apoptosis in the spheroids post drug treatments. We determined the kinetics of apoptosis induction using AnnexinV/PI staining. Drug-induced apoptosis was readily detected in the LNCaP spheroids treated with mono and dual drug combinations. In concurrence with the previous results, the combination of the three synergistic drugs with 116-9e displayed enhanced apoptosis as compared to the single drug treatment whereas spheroids treated with the 3 antagonistic drugs showed little or no difference in the rate of apoptosis as compared to the dual drug combination with 116-9e (Figure 4B).

DISCUSSION

Although inhibitors of Hsp70 and Hsp90 have been developed for research purposes, conversion of these molecules for use in patient treatment have been hampered by toxicity issues [4]. We undertook this study to resolve conflicting literature on whether inhibiting HDJ2, a co-chaperone of Hsp70 may be useful as a novel anticancer strategy. Our bioinformatic analysis of HDJ2 expression and mutation clearly identify HDJ2 as being highly altered in a range of cancers, particularly in Prostate Cancer. This data in conjunction with a recent finding that Hsp40 is involved in functional regulation of ARv [22] makes HDJ2 inhibition an ideal choice as a novel therapeutic target in Prostate Cancer.

Chemogenomic screening of knockout cell lines produces both useful mechanistic and translational understanding of protein function. In this study, loss of HDJ2 increased the potency of a substantial number (31%) of clinically used anticancer drugs.

Hsp70 activates many proteins involved in the DNA damage response and DNA repair pathways (DDR). These include ATM, APE1, PARP1, XRCC1, LIG3, MSH2, MLH1 and Apollo [49-51]. In addition, studies from our group have established roles for both Hsp70 and HDJ2 in stability of the RNR complex [13, 50, 52]. As such, we would expect a high degree of synergy between loss of HDJ2 function and the DNA damage response/repair pathways. Correspondingly, around 20 commonly used anticancer DNA damage and Repair (DDR) inhibitors were found to be synergistic with loss of HDJ2. These included 5-fluorouracil (5-FU) and premetrexed, widely used anticancer drugs whose metabolites are incorporated into both DNA and RNA in addition to inhibiting thymidylate synthase [53]. Here we validated synergy with the RNR inhibitor clofarabine. Clofarabine is phosphorylated intracellularly to form cytotoxic active 5'-triphosphate metabolite, which inhibits the enzymatic activities of RNR and DNA polymerase, resulting in inhibition of DNA synthesis and repair[54]. In addition, we also identified PARP inhibitors olaparib and niraparib and the topoisomerase inhibitors etoposide, teniposide, valrubicin and dexrazoxane to have increased potency in our screen.

While most DDR inhibitors displayed increased potency with HDJ2 depletion, four of them were antagonistic to loss of HDJ2. These include topoisomerase inhibitors and nucleic acid synthesis inhibitors such as trifluridine, irinotecan, epirubicin (4'-epi-isomer of the antibiotic doxorubicin) and idarubicin (4-demethoxy analogue of daunorubicin)[55]. While at first these results seem paradoxical, it is worth noting that inrinotecan is a type I

topoisomerase inhibitor, whereas Etoposide inhibits the type II class. It may be that Hsp70 and HDJ2 play different regulatory roles in the stabilization and activation of these related proteins. It should be noted that both idarubicin and epirubicin trigger TOPII-mediated DNA cleavage. The effects of these molecules may be prevented if HDJ2 alters the function of TOPII.

In addition to DDR, HDJ2 is also involved in signal transduction, with previous reports indicating that the yeast homologue of HDJ2 (Ydj1) is critical for supporting the integrity of kinase signaling networks [56]. HDJ2 is mobilized to specific sites within the nucleus in response to inappropriate targeting or folding of specific mutant receptors. HDJ2 overexpression ameliorates defective transactivation and trans repression activity of mutant Glucocorticoid receptors [57]. In line with the previous studies, we found that a handful of Receptor Tyrosine kinase inhibitors were synergistic with HDJ2 depletion. These included Vascular endothelial growth factor receptor (VEGFR) inhibitors such as sunitinib, cabozantinib, lenvatinib and pazopanib. Interestingly, randomized phase III clinical trials are being conducted to validate the efficacy of Cabozantinib in heavily pretreated prostate cancer patients [58]. One implication from our study is that HDJ2 inhibition might significantly enhance the effect of cabozantinib monotherapy.

Strikingly, some of the kinase inhibitors were antagonistic to HDJ2 depletion. These include VEGFR inhibitors such as regorafenib and sorafenib. This disparity can be explained by the different target receptors and mechanisms of action of these drugs. Interestingly, recent studies indicated that these small molecule inhibitors exhibit off-target effects. Some of these drugs are misidentified and mischaracterized for their target

317 specific inhibition, which has contributed to the high failure rate of these drugs in treatment
318 of cancer patients [59].
319 Other than its role in signal transduction, HDJ2 is also important for maintaining the
320 cellular cytoskeleton. Previous studies have suggested that YDJ1 (yeast homolog of
321 HDJ2) is important for the proper assembly of microtubules [60, 61]. Another report
322 showed that HDJ2 depletion causes relocation of N-cadherin and enhanced activity of
323 metalloproteinases. This leads to changes in the actin cytoskeleton indicating that HDJ2
324 is important for prevention of the amoeboid-like transition of tumor cells [62]. These
325 studies indicated the involvement of HDJ2 in maintaining cytoskeletal organization. We
326 found 3 anticancer drugs targeting the cytoskeleton to be synergistic with HDJ2 depletion,
327 including vinblastine sulfate (cytoskeletal inhibitor that disrupts microtubule formation
328 during mitosis and interferes with glutamic acid metabolism), estramustine (binds to
329 microtubule-associated proteins (MAPs) and inhibits microtubule dynamics) and
330 ixabepilone (promotes tubulin polymerization and microtubule stabilization, thereby
331 arresting cells in the G2-M phase [63].
332 Strikingly, two of the tubulin inhibitors were found to be antagonistic to HDJ2 depletion.
333 These include paclitaxel and ixabepilone. Paclitaxel inhibits the disassembly of
334 microtubules resulting in the inhibition of cell division whereas Ixabepilone promotes
335 tubulin polymerization and microtubule stabilization, arresting cells in the G2-M phase of
336 the cell cycle [63]. This discrepancy again implies that these cytoskeletal inhibitors might
337 have off target effects due to their mischaracterization [59].
338 Epigenetic modifying drugs display substantially modified potency depending on cellular
339 HDJ2 status. While previous studies have indicated the association between proteomic

changes and histone PTMs in response to Hsp90 inhibitor treatment in bladder carcinoma cells, no such association has been shown for HDJ2 and Histone PTMs [64]. Interestingly, vorinostat was the only drug that was synergistic to HDJ2 inhibition. It is a histone deacetylase inhibitor that binds to the catalytic domain of the histone deacetylases (HDACs) [65]. However, we identified two histone deacetylase inhibitor drugs to be antagonistic to HDJ2 depletion**:** panobinostat and romidepsin inhibit histone deacetylase (HDAC), inducing hyperacetylation of core histone proteins, which may result in modulation of cell cycle protein expression, cell cycle arrest in the G2/M phase and apoptosis [66]. This is the first study that indicates an association between histone PTMs and HDJ2. While these findings require further investigation, it is possible that HDJ2 regulates histone properties. Interestingly, both of the protein synthesis inhibitors (bortezomib and omacetaxine) in our screen were antagonistic to HDJ2 depletion [67]. We confirmed that omacetaxine (protein biosynthesis inhibitor) displayed reduced potency upon inhibition of HDJ2 [42].

Several important conclusions can be inferred from the data presented here. Firstly, our HTS screening method might be useful in the selection of drugs for individual patients in future studies, since the drug sensitivity of cancer cells is dependent on HDJ2 expression. For example, compounds that belong to the same category such as sunitinib and sorafenib may behave differently upon HDJ2 deletion.

Finally, in addition to intra-pathway synergistic combinations (VEGFRi, MAPKi pathway inhibitors, and DNA damage/cell-cycle checkpoint pathway combinations), which is consistent with a wealth of publications demonstrating intrapathway synergy [68, 69], we also discovered novel inter-pathway combinations of HDJ2. This study describes

363 promising results and indicates an integrative approach based on HTS which has
364 potential to govern cancer patient treatment by combination therapy. Taken together, this
365 study suggests a potential Precision Medicine approach that has the potential to inform
366 anticancer strategy based on patient HDJ2 status.

367

368 **Acknowledgements**

369 The authors thank NIH for providing materials used in this study and J. Gestwicki, D.
370 Dreau and T. Erick for helpful comments. This project was supported by NCI
371 R15CA208773 and Grant-In-Aid of Research from Sigma Xi (G2018031591887158), The
372 Scientific Research Society.

373

374 **References**

375 1. Rosenzweig R, Nillegoda NB, Mayer MP, Bukau B. The Hsp70 chaperone network. Nat
376 Rev Mol Cell Biol. 2019. Epub 2019/06/30. doi: 10.1038/s41580-019-0133-3. PubMed PMID:
377 31253954.
378 2. Ciocca DR, Calderwood SK. Heat shock proteins in cancer: diagnostic, prognostic,
379 predictive, and treatment implications. Cell Stress Chaperones. 2005;10(2):86-103. Epub
380 2005/07/26. doi: 10.1379/csc-99r.1. PubMed PMID: 16038406; PubMed Central PMCID:
381 PMCPMC1176476.
382 3. Gestwicki JE, Shao H. Inhibitors and chemical probes for molecular chaperone networks.
383 J Biol Chem. 2019;294(6):2151-61. Epub 2018/09/15. doi: 10.1074/jbc.TM118.002813. PubMed
384 PMID: 30213856; PubMed Central PMCID: PMCPMC6369302.
385 4. Evans CG, Chang L, Gestwicki JE. Heat shock protein 70 (hsp70) as an emerging drug
386 target. J Med Chem. 2010;53(12):4585-602. Epub 2010/03/26. doi: 10.1021/jm100054f. PubMed
387 PMID: 20334364; PubMed Central PMCID: PMCPMC2895966.
388 5. Bertelsen EB, Chang L, Gestwicki JE, Zuiderweg ER. Solution conformation of wild-type
389 E. coli Hsp70 (DnaK) chaperone complexed with ADP and substrate. Proc Natl Acad Sci U S A.
390 2009;106(21):8471-6. Epub 2009/05/15. doi: 10.1073/pnas.0903503106. PubMed PMID:
391 19439666; PubMed Central PMCID: PMCPMC2689011.
392 6. Kampinga HH, Craig EA. The HSP70 chaperone machinery: J proteins as drivers of
393 functional specificity. Nat Rev Mol Cell Biol. 2010;11(8):579-92. Epub 2010/07/24. doi:
394 10.1038/nrm2941. PubMed PMID: 20651708; PubMed Central PMCID: PMCPMC3003299.
395 7. Craig EA, Marszalek J. How Do J-Proteins Get Hsp70 to Do So Many Different Things?
396 Trends Biochem Sci. 2017;42(5):355-68. Epub 2017/03/21. doi: 10.1016/j.tibs.2017.02.007.
397 PubMed PMID: 28314505; PubMed Central PMCID: PMCPMC5409888.

8. Hageman J, van Waarde MA, Zylicz A, Walerych D, Kampinga HH. The diverse members of the mammalian HSP70 machine show distinct chaperone-like activities. Biochem J. 2011;435(1):127-42. Epub 2011/01/15. doi: 10.1042/BJ20101247. PubMed PMID: 21231916.
9. Assimon VA, Gillies AT, Rauch JN, Gestwicki JE. Hsp70 protein complexes as drug targets. Curr Pharm Des. 2013;19(3):404-17. Epub 2012/08/28. doi: 10.2174/138161213804143699. PubMed PMID: 22920901; PubMed Central PMCID: PMCPMC3593251.
10. Walton-Diaz A, Khan S, Bourboulia D, Trepel JB, Neckers L, Mollapour M. Contributions of co-chaperones and post-translational modifications towards Hsp90 drug sensitivity. Future Med Chem. 2013;5(9):1059-71. Epub 2013/06/06. doi: 10.4155/fmc.13.88. PubMed PMID: 23734688.
11. Taylor IR, Dunyak BM, Komiyama T, Shao H, Ran X, Assimon VA, et al. High-throughput screen for inhibitors of protein-protein interactions in a reconstituted heat shock protein 70 (Hsp70) complex. J Biol Chem. 2018;293(11):4014-25. Epub 2018/02/08. doi: 10.1074/jbc.RA117.001575. PubMed PMID: 29414793; PubMed Central PMCID: PMCPMC5857975.
12. Nitika, Truman AW. Cracking the Chaperone Code: Cellular Roles for Hsp70 Phosphorylation. Trends Biochem Sci. 2017;42(12):932-5. Epub 2017/11/06. doi: 10.1016/j.tibs.2017.10.002. PubMed PMID: 29102083; PubMed Central PMCID: PMCPMC5701876.
13. Sluder IT, Nitika, Knighton LE, Truman AW. The Hsp70 co-chaperone Ydj1/HDJ2 regulates ribonucleotide reductase activity. PLoS Genet. 2018;14(11):e1007462. Epub 2018/11/20. doi: 10.1371/journal.pgen.1007462. PubMed PMID: 30452489; PubMed Central PMCID: PMCPMC6277125.
14. Truman AW, Kristjansdottir K, Wolfgeher D, Hasin N, Polier S, Zhang H, et al. CDK-dependent Hsp70 Phosphorylation controls G1 cyclin abundance and cell-cycle progression. Cell. 2012;151(6):1308-18. Epub 2012/12/12. doi: 10.1016/j.cell.2012.10.051. PubMed PMID: 23217712; PubMed Central PMCID: PMCPMC3778871.
15. Woodford MR, Dunn DM, Blanden AR, Capriotti D, Loiselle D, Prodromou C, et al. The FNIP co-chaperones decelerate the Hsp90 chaperone cycle and enhance drug binding. Nat Commun. 2016;7:12037. Epub 2016/06/30. doi: 10.1038/ncomms12037. PubMed PMID: 27353360; PubMed Central PMCID: PMCPMC4931344.
16. Woodford MR, Dunn D, Miller JB, Jamal S, Neckers L, Mollapour M. Impact of Posttranslational Modifications on the Anticancer Activity of Hsp90 Inhibitors. Adv Cancer Res. 2016;129:31-50. Epub 2016/02/27. doi: 10.1016/bs.acr.2015.09.002. PubMed PMID: 26916000.
17. Woodford MR, Truman AW, Dunn DM, Jensen SM, Cotran R, Bullard R, et al. Mps1 Mediated Phosphorylation of Hsp90 Confers Renal Cell Carcinoma Sensitivity and Selectivity to Hsp90 Inhibitors. Cell Rep. 2016;14(4):872-84. Epub 2016/01/26. doi: 10.1016/j.celrep.2015.12.084. PubMed PMID: 26804907; PubMed Central PMCID: PMCPMC4887101.
18. Dushukyan N, Dunn DM, Sager RA, Woodford MR, Loiselle DR, Daneshvar M, et al. Phosphorylation and Ubiquitination Regulate Protein Phosphatase 5 Activity and Its Prosurvival Role in Kidney Cancer. Cell Rep. 2017;21(7):1883-95. Epub 2017/11/16. doi: 10.1016/j.celrep.2017.10.074. PubMed PMID: 29141220; PubMed Central PMCID: PMCPMC5699234.
19. Nitika, Truman AW. Endogenous epitope tagging of heat shock protein 70 isoform Hsc70 using CRISPR/Cas9. Cell Stress Chaperones. 2018;23(3):347-55. Epub 2017/09/26. doi: 10.1007/s12192-017-0845-2. PubMed PMID: 28944418; PubMed Central PMCID: PMCPMC5904078.
20. Parrales A, Ranjan A, Iyer SV, Padhye S, Weir SJ, Roy A, et al. DNAJA1 controls the fate of misfolded mutant p53 through the mevalonate pathway. Nat Cell Biol. 2016;18(11):1233-43.

448 Epub 2016/10/28. doi: 10.1038/ncb3427. PubMed PMID: 27775703; PubMed Central PMCID:
449 PMCPMC5340314.
450 21. Stark JL, Mehla K, Chaika N, Acton TB, Xiao R, Singh PK, et al. Structure and function of
451 human DnaJ homologue subfamily a member 1 (DNAJA1) and its relationship to pancreatic
452 cancer. Biochemistry. 2014;53(8):1360-72. Epub 2014/02/12. doi: 10.1021/bi401329a. PubMed
453 PMID: 24512202; PubMed Central PMCID: PMCPMC3985919.
454 22. Moses MA, Kim YS, Rivera-Marquez GM, Oshima N, Watson MJ, Beebe KE, et al.
455 Targeting the Hsp40/Hsp70 Chaperone Axis as a Novel Strategy to Treat Castration-Resistant
456 Prostate Cancer. Cancer Res. 2018;78(14):4022-35. Epub 2018/05/17. doi: 10.1158/0008-
457 5472.CAN-17-3728. PubMed PMID: 29764864; PubMed Central PMCID: PMCPMC6050126.
458 23. O'Neil J, Benita Y, Feldman I, Chenard M, Roberts B, Liu Y, et al. An Unbiased Oncology
459 Compound Screen to Identify Novel Combination Strategies. Mol Cancer Ther. 2016;15(6):1155-
460 62. Epub 2016/03/18. doi: 10.1158/1535-7163.MCT-15-0843. PubMed PMID: 26983881.
461 24. Palmer AC, Sorger PK. Combination Cancer Therapy Can Confer Benefit via Patient-to-
462 Patient Variability without Drug Additivity or Synergy. Cell. 2017;171(7):1678-91 e13. Epub
463 2017/12/16. doi: 10.1016/j.cell.2017.11.009. PubMed PMID: 29245013; PubMed Central PMCID:
464 PMCPMC5741091.
465 25. Ding KF, Petricoin EF, Finlay D, Yin H, Hendricks WPD, Sereduk C, et al. Nonlinear mixed
466 effects dose response modeling in high throughput drug screens: application to melanoma cell
467 line analysis. Oncotarget. 2018;9(4):5044-57. Epub 2018/02/13. doi: 10.18632/oncotarget.23495.
468 PubMed PMID: 29435161; PubMed Central PMCID: PMCPMC5797032.
469 26. Koh SB, Wallez Y, Dunlop CR, Bernaldo de Quiros Fernandez S, Bapiro TE, Richards
470 FM, et al. Mechanistic Distinctions between CHK1 and WEE1 Inhibition Guide the Scheduling of
471 Triple Therapy with Gemcitabine. Cancer Res. 2018;78(11):3054-66. Epub 2018/05/08. doi:
472 10.1158/0008-5472.CAN-17-3932. PubMed PMID: 29735549; PubMed Central PMCID:
473 PMCPMC5985963.
474 27. Jones LH, Bunnage ME. Applications of chemogenomic library screening in drug
475 discovery. Nat Rev Drug Discov. 2017;16(4):285-96. Epub 2017/01/21. doi:
476 10.1038/nrd.2016.244. PubMed PMID: 28104905.
477 28. Chou TC. Theoretical basis, experimental design, and computerized simulation of
478 synergism and antagonism in drug combination studies. Pharmacol Rev. 2006;58(3):621-81. doi:
479 10.1124/pr.58.3.10. PubMed PMID: 16968952.
480 29. Wu J, Liu T, Rios Z, Mei Q, Lin X, Cao S. Heat Shock Proteins and Cancer. Trends
481 Pharmacol Sci. 2017;38(3):226-56. Epub 2016/12/26. doi: 10.1016/j.tips.2016.11.009. PubMed
482 PMID: 28012700.
483 30. Murphy ME. The HSP70 family and cancer. Carcinogenesis. 2013;34(6):1181-8. Epub
484 2013/04/09. doi: 10.1093/carcin/bgt111. PubMed PMID: 23563090; PubMed Central PMCID:
485 PMCPMC3670260.
486 31. Gao J, Aksoy BA, Dogrusoz U, Dresdner G, Gross B, Sumer SO, et al. Integrative analysis
487 of complex cancer genomics and clinical profiles using the cBioPortal. Sci Signal.
488 2013;6(269):pl1. Epub 2013/04/04. doi: 10.1126/scisignal.2004088. PubMed PMID: 23550210;
489 PubMed Central PMCID: PMCPMC4160307.
490 32. Cerami E, Gao J, Dogrusoz U, Gross BE, Sumer SO, Aksoy BA, et al. The cBio cancer
491 genomics portal: an open platform for exploring multidimensional cancer genomics data. Cancer
492 Discov. 2012;2(5):401-4. Epub 2012/05/17. doi: 10.1158/2159-8290.CD-12-0095. PubMed PMID:
493 22588877; PubMed Central PMCID: PMCPMC3956037.
494 33. Wang CC, Liao YP, Mischel PS, Iwamoto KS, Cacalano NA, McBride WH. HDJ-2 as a
495 target for radiosensitization of glioblastoma multiforme cells by the farnesyltransferase inhibitor
496 R115777 and the role of the p53/p21 pathway. Cancer Res. 2006;66(13):6756-62. Epub
497 2006/07/05. doi: 10.1158/0008-5472.CAN-06-0185. PubMed PMID: 16818651.

34. Wong CC, Cheng KW, Rigas B. Preclinical predictors of anticancer drug efficacy: critical assessment with emphasis on whether nanomolar potency should be required of candidate agents. J Pharmacol Exp Ther. 2012;341(3):572-8. Epub 2012/03/27. doi: 10.1124/jpet.112.191957. PubMed PMID: 22448039; PubMed Central PMCID: PMCPMC3362883.
35. Wisen S, Bertelsen EB, Thompson AD, Patury S, Ung P, Chang L, et al. Binding of a small molecule at a protein-protein interface regulates the chaperone activity of hsp70-hsp40. ACS Chem Biol. 2010;5(6):611-22. Epub 2010/05/21. doi: 10.1021/cb1000422. PubMed PMID: 20481474; PubMed Central PMCID: PMCPMC2950966.
36. Wisitpitthaya S, Zhao Y, Long MJ, Li M, Fletcher EA, Blessing WA, et al. Cladribine and Fludarabine Nucleotides Induce Distinct Hexamers Defining a Common Mode of Reversible RNR Inhibition. ACS Chem Biol. 2016;11(7):2021-32. Epub 2016/05/10. doi: 10.1021/acschembio.6b00303. PubMed PMID: 27159113; PubMed Central PMCID: PMCPMC4946967.
37. Xiang Q, Chen W, Ren M, Wang J, Zhang H, Deng DY, et al. Cabozantinib suppresses tumor growth and metastasis in hepatocellular carcinoma by a dual blockade of VEGFR2 and MET. Clin Cancer Res. 2014;20(11):2959-70. Epub 2014/04/05. doi: 10.1158/1078-0432.CCR-13-2620. PubMed PMID: 24700742.
38. Augustin A, Lamerz J, Meistermann H, Golling S, Scheiblich S, Hermann JC, et al. Quantitative chemical proteomics profiling differentiates erlotinib from gefitinib in EGFR wild-type non-small cell lung carcinoma cell lines. Mol Cancer Ther. 2013;12(4):520-9. Epub 2013/02/02. doi: 10.1158/1535-7163.MCT-12-0880. PubMed PMID: 23371860.
39. Wu CC, Li TK, Farh L, Lin LY, Lin TS, Yu YJ, et al. Structural basis of type II topoisomerase inhibition by the anticancer drug etoposide. Science. 2011;333(6041):459-62. Epub 2011/07/23. doi: 10.1126/science.1204117. PubMed PMID: 21778401.
40. Senra JM, Telfer BA, Cherry KE, McCrudden CM, Hirst DG, O'Connor MJ, et al. Inhibition of PARP-1 by olaparib (AZD2281) increases the radiosensitivity of a lung tumor xenograft. Mol Cancer Ther. 2011;10(10):1949-58. Epub 2011/10/06. doi: 10.1158/1535-7163.MCT-11-0278. PubMed PMID: 21825006; PubMed Central PMCID: PMCPMC3192032.
41. Dudgeon C, Peng R, Wang P, Sebastiani A, Yu J, Zhang L. Inhibiting oncogenic signaling by sorafenib activates PUMA via GSK3beta and NF-kappaB to suppress tumor cell growth. Oncogene. 2012;31(46):4848-58. Epub 2012/01/31. doi: 10.1038/onc.2011.644. PubMed PMID: 22286758; PubMed Central PMCID: PMCPMC3342476.
42. Gandhi V, Plunkett W, Cortes JE. Omacetaxine: a protein translation inhibitor for treatment of chronic myelogenous leukemia. Clin Cancer Res. 2014;20(7):1735-40. Epub 2014/02/07. doi: 10.1158/1078-0432.CCR-13-1283. PubMed PMID: 24501394; PubMed Central PMCID: PMCPMC4048124.
43. Hevener K, Verstak TA, Lutat KE, Riggsbee DL, Mooney JW. Recent developments in topoisomerase-targeted cancer chemotherapy. Acta Pharm Sin B. 2018;8(6):844-61. Epub 2018/12/07. doi: 10.1016/j.apsb.2018.07.008. PubMed PMID: 30505655; PubMed Central PMCID: PMCPMC6251812.
44. Chou TC. Drug combination studies and their synergy quantification using the Chou-Talalay method. Cancer Res. 2010;70(2):440-6. Epub 2010/01/14. doi: 10.1158/0008-5472.CAN-09-1947. PubMed PMID: 20068163.
45. Vlachogiannis G, Hedayat S, Vatsiou A, Jamin Y, Fernandez-Mateos J, Khan K, et al. Patient-derived organoids model treatment response of metastatic gastrointestinal cancers. Science. 2018;359(6378):920-6. Epub 2018/02/24. doi: 10.1126/science.aao2774. PubMed PMID: 29472484; PubMed Central PMCID: PMCPMC6112415.
46. Prasad V, Fojo T, Brada M. Precision oncology: origins, optimism, and potential. Lancet Oncol. 2016;17(2):e81-e6. Epub 2016/02/13. doi: 10.1016/S1470-2045(15)00620-8. PubMed PMID: 26868357.

549 47. Nyga A, Cheema U, Loizidou M. 3D tumour models: novel in vitro approaches to cancer
550 studies. J Cell Commun Signal. 2011;5(3):239-48. Epub 2011/04/19. doi: 10.1007/s12079-011-
551 0132-4. PubMed PMID: 21499821; PubMed Central PMCID: PMCPMC3145874.
552 48. Pickl M, Ries CH. Comparison of 3D and 2D tumor models reveals enhanced HER2
553 activation in 3D associated with an increased response to trastuzumab. Oncogene.
554 2009;28(3):461-8. Epub 2008/11/04. doi: 10.1038/onc.2008.394. PubMed PMID: 18978815.
555 49. Sottile ML, Nadin SB. Heat shock proteins and DNA repair mechanisms: an updated
556 overview. Cell Stress Chaperones. 2018;23(3):303-15. Epub 2017/09/28. doi: 10.1007/s12192-
557 017-0843-4. PubMed PMID: 28952019; PubMed Central PMCID: PMCPMC5904076.
558 50. Knighton LE, Delgado LE, Truman AW. Novel insights into molecular chaperone
559 regulation of ribonucleotide reductase. Curr Genet. 2019;65(2):477-82. Epub 2018/12/07. doi:
560 10.1007/s00294-018-0916-7. PubMed PMID: 30519713; PubMed Central PMCID:
561 PMCPMC6421096.
562 51. Dubrez L, Causse S, Borges Bonan N, Dumetier B, Garrido C. Heat-shock proteins:
563 chaperoning DNA repair. Oncogene. 2019. Epub 2019/09/22. doi: 10.1038/s41388-019-1016-y.
564 PubMed PMID: 31541194.
565 52. Truman AW, Kristjansdottir K, Wolfgeher D, Ricco N, Mayampurath A, Volchenboum SL,
566 et al. Quantitative proteomics of the yeast Hsp70/Hsp90 interactomes during DNA damage reveal
567 chaperone-dependent regulation of ribonucleotide reductase. Journal of proteomics.
568 2015;112:285-300. Epub 2014/12/03. doi: 10.1016/j.jprot.2014.09.028. PubMed PMID:
569 25452130; PubMed Central PMCID: PMCPMC4485990.
570 53. Longley DB, Harkin DP, Johnston PG. 5-fluorouracil: mechanisms of action and clinical
571 strategies. Nat Rev Cancer. 2003;3(5):330-8. Epub 2003/05/02. doi: 10.1038/nrc1074. PubMed
572 PMID: 12724731.
573 54. Huguet F, Leguay T, Raffoux E, Rousselot P, Vey N, Pigneux A, et al. Clofarabine for the
574 treatment of adult acute lymphoid leukemia: the Group for Research on Adult Acute
575 Lymphoblastic Leukemia intergroup. Leuk Lymphoma. 2015;56(4):847-57. Epub 2014/07/06. doi:
576 10.3109/10428194.2014.887708. PubMed PMID: 24996442.
577 55. Deng S, Yan T, Jendrny C, Nemecek A, Vincetic M, Godtel-Armbrust U, et al.
578 Dexrazoxane may prevent doxorubicin-induced DNA damage via depleting both topoisomerase
579 II isoforms. BMC Cancer. 2014;14:842. Epub 2014/11/20. doi: 10.1186/1471-2407-14-842.
580 PubMed PMID: 25406834; PubMed Central PMCID: PMCPMC4242484.
581 56. Gillies AT, Taylor R, Gestwicki JE. Synthetic lethal interactions in yeast reveal functional
582 roles of J protein co-chaperones. Mol Biosyst. 2012;8(11):2901-8. Epub 2012/08/02. doi:
583 10.1039/c2mb25248a. PubMed PMID: 22851130; PubMed Central PMCID: PMCPMC3463740.
584 57. Tang Y, Ramakrishnan C, Thomas J, DeFranco DB. A role for HDJ-2/HSDJ in correcting
585 subnuclear trafficking, transactivation, and transrepression defects of a glucocorticoid receptor
586 zinc finger mutant. Mol Biol Cell. 1997;8(5):795-809. Epub 1997/05/01. PubMed PMID: 9168467;
587 PubMed Central PMCID: PMCPMC276130.
588 58. Grullich C. Cabozantinib: a MET, RET, and VEGFR2 tyrosine kinase inhibitor. Recent
589 Results Cancer Res. 2014;201:207-14. Epub 2014/04/24. doi: 10.1007/978-3-642-54490-3_12.
590 PubMed PMID: 24756794.
591 59. Lin A, Giuliano CJ, Palladino A, John KM, Abramowicz C, Yuan ML, et al. Off-target toxicity
592 is a common mechanism of action of cancer drugs undergoing clinical trials. Sci Transl Med.
593 2019;11(509). Epub 2019/09/13. doi: 10.1126/scitranslmed.aaw8412. PubMed PMID: 31511426.
594 60. Oka M, Nakai M, Endo T, Lim CR, Kimata Y, Kohno K. Loss of Hsp70-Hsp40 chaperone
595 activity causes abnormal nuclear distribution and aberrant microtubule formation in M-phase of
596 Saccharomyces cerevisiae. J Biol Chem. 1998;273(45):29727-37. Epub 1998/10/29. doi:
597 10.1074/jbc.273.45.29727. PubMed PMID: 9792686.
598 61. Silflow CD, Sun X, Haas NA, Foley JW, Lefebvre PA. The Hsp70 and Hsp40 chaperones
599 influence microtubule stability in Chlamydomonas. Genetics. 2011;189(4):1249-60. Epub

2011/09/24. doi: 10.1534/genetics.111.133587. PubMed PMID: 21940683; PubMed Central PMCID: PMCPMC3241413.
62. Meshalkina DA, Shevtsov MA, Dobrodumov AV, Komarova EY, Voronkina IV, Lazarev VF, et al. Knock-down of Hdj2/DNAJA1 co-chaperone results in an unexpected burst of tumorigenicity of C6 glioblastoma cells. Oncotarget. 2016;7(16):22050-63. Epub 2016/03/10. doi: 10.18632/oncotarget.7872. PubMed PMID: 26959111; PubMed Central PMCID: PMCPMC5008343.
63. Cobham MV, Donovan D. Ixabepilone: a new treatment option for the management of taxane-resistant metastatic breast cancer. Cancer Manag Res. 2009;1:69-77. Epub 2009/01/01. PubMed PMID: 21188125; PubMed Central PMCID: PMCPMC3004658.
64. Li QQ, Hao JJ, Zhang Z, Krane LS, Hammerich KH, Sanford T, et al. Proteomic analysis of proteome and histone post-translational modifications in heat shock protein 90 inhibition-mediated bladder cancer therapeutics. Sci Rep. 2017;7(1):201. Epub 2017/03/17. doi: 10.1038/s41598-017-00143-6. PubMed PMID: 28298630; PubMed Central PMCID: PMCPMC5427839.
65. Mettananda S, Yasara N, Fisher CA, Taylor S, Gibbons R, Higgs D. Synergistic silencing of alpha-globin and induction of gamma-globin by histone deacetylase inhibitor, vorinostat as a potential therapy for beta-thalassaemia. Sci Rep. 2019;9(1):11649. Epub 2019/08/14. doi: 10.1038/s41598-019-48204-2. PubMed PMID: 31406232; PubMed Central PMCID: PMCPMC6690964.
66. Eckschlager T, Plch J, Stiborova M, Hrabeta J. Histone Deacetylase Inhibitors as Anticancer Drugs. Int J Mol Sci. 2017;18(7). Epub 2017/07/04. doi: 10.3390/ijms18071414. PubMed PMID: 28671573; PubMed Central PMCID: PMCPMC5535906.
67. Bewersdorf JP, Shallis R, Stahl M, Zeidan AM. Epigenetic therapy combinations in acute myeloid leukemia: what are the options? Ther Adv Hematol. 2019;10:2040620718816698. Epub 2019/02/06. doi: 10.1177/2040620718816698. PubMed PMID: 30719265; PubMed Central PMCID: PMCPMC6348528.
68. Johnson N, Shapiro GI. Cyclin-dependent kinases (cdks) and the DNA damage response: rationale for cdk inhibitor-chemotherapy combinations as an anticancer strategy for solid tumors. Expert Opin Ther Targets. 2010;14(11):1199-212. Epub 2010/10/12. doi: 10.1517/14728222.2010.525221. PubMed PMID: 20932174; PubMed Central PMCID: PMCPMC3957489.
69. Karakashev S, Zhu H, Yokoyama Y, Zhao B, Fatkhutdinov N, Kossenkov AV, et al. BET Bromodomain Inhibition Synergizes with PARP Inhibitor in Epithelial Ovarian Cancer. Cell Rep. 2017;21(12):3398-405. Epub 2017/12/21. doi: 10.1016/j.celrep.2017.11.095. PubMed PMID: 29262321; PubMed Central PMCID: PMCPMC5745042.

Figure legends.

Figure 1. HDJ2 is altered in cancer. (A) Prevalence of HDJ2 alterations in various cancer genomes analyzed via the cBioPortal. Red bar, amplification. Blue bar, homozygous deletion. Green square, missense mutation. Purple square, Fusion. (B)

642 HDJ2 mRNA expression in tumor determined via cBioPortal. P-value for a gene
643 represents its P-value for the median-ranked analysis.
644
645 **Figure 2. Sensitivity of WT and HDJ2 knockout cells to the NIH Approved Oncology**
646 **Collection.** (A) Workflow of high-throughput cell-based screen. (B) A collection of 132
647 drugs were screened at 50μmol/L with Wild-type and HDJ2 KO cells. Results are the
648 average of at least triplicates and error is SEM. The dotted lines represent an interaction
649 change of up or down two-fold. The dotted lines represent an interaction change of
650 $Log_2 > 1.5$ or $Log_2 < -1.5$.The effect of drug combination are colored according to
651 significant upregulation and downregulation: red (synergistic), green (antagonistic) or
652 black (no significant change). C) & D) Drug ontology of synergistic and antagonistic hits
653 based on the pathways affected by the approved oncology drugs in the screen.
654
655 **Figure 3. Drug interaction between 116-9e (HDJ2 inhibitor) and selected hits.**
656 LNCaP cells were treated with different concentration of Cabozantinib, Clofarabine,
657 Vinblastine, Idarubicin, Omacetaxine and Sorafenib with or without 116-9e for 72 hours
658 in RPMI-1640 medium containing 10% FBS. Each point is the mean ± SD for three
659 independent experiments. Growth inhibition was determined using Cell Titer-Glo assay.
660 Combination Index (CI, measure of drug synergy) was determined using Chou-Talalay
661 method via Compusyn software. CI values of <1 indicate drug synergy.
662
663 **Figure 4. Effect of combination treatments on prostate cancer spheroids.**
664 A. Cells were plated on Matrigel coated 24 well plates. Six drugs (Cabozantinib,

Clofarabine, Vinblastine, Idarubicin, Omacetaxine and Sorafenib) were tested in triplicates for prostate cancer spheroids. The pictures are representative images as acquired using EVOS cell imager. B. Proliferation of spheroids treated with Cabozantinib (CBZ), Clofarabine (CFB), Vinblastine (VBT), Idarubicin (IRB), Omacetaxine (OAT) and Sorafenib (SRN) measured using AnnexinV/PI staining.

Graphical Abstract

HDJ2 knockout or inhibition via small molecule impacts cellular resistance to anticancer therapeutics.

Supplementary Data

Supplementary Table 1. Hits identified in combination screen with simultaneous treatment of Approved oncology drugs with HDJ2 Knockout HAP1 cell lines.

Prostate Cancer

Hdj2 KO

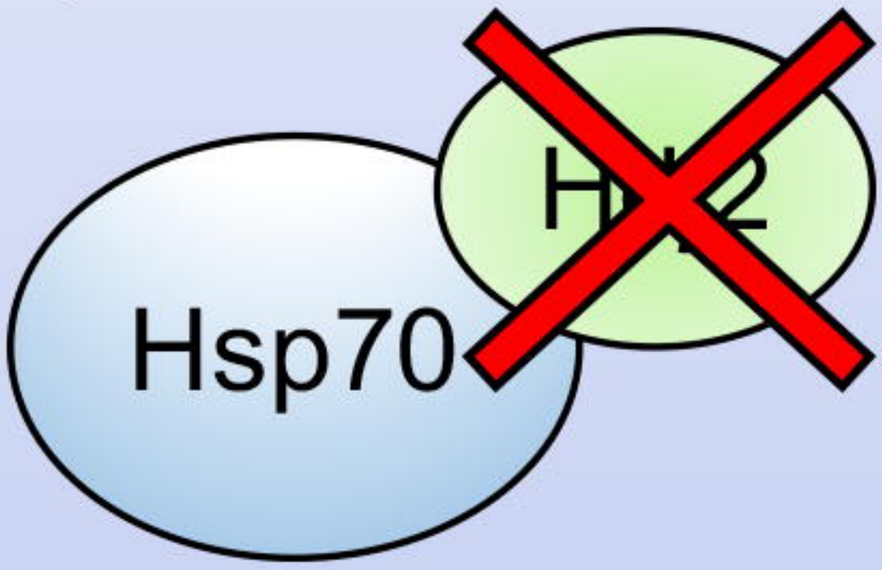

OR

116-9e

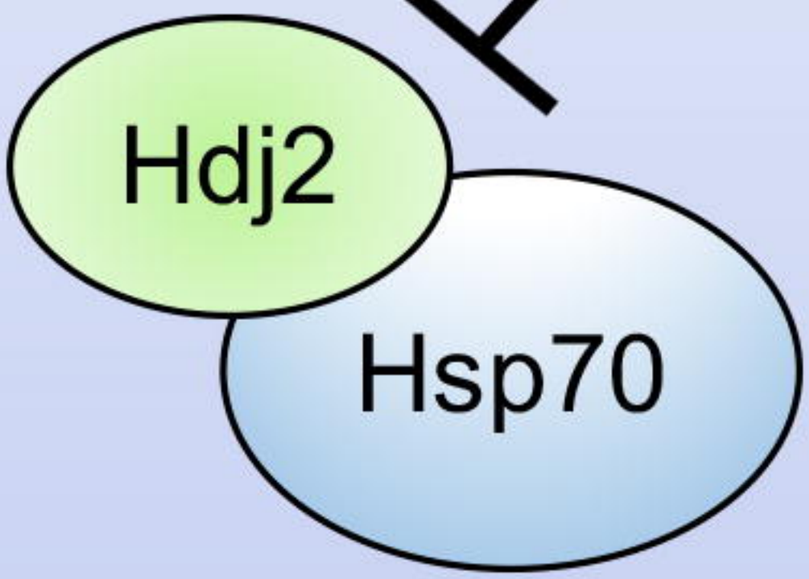

Increased Sensitivity to:

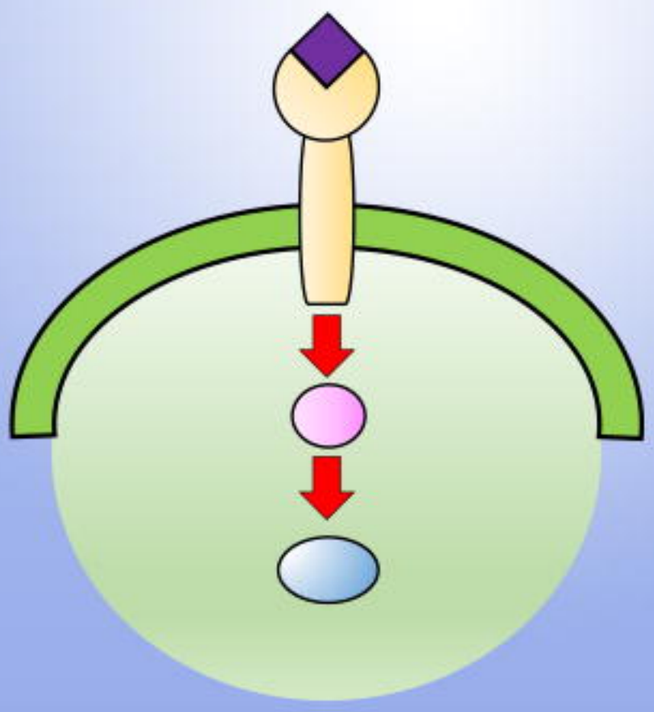

Decreased Sensitivity to:

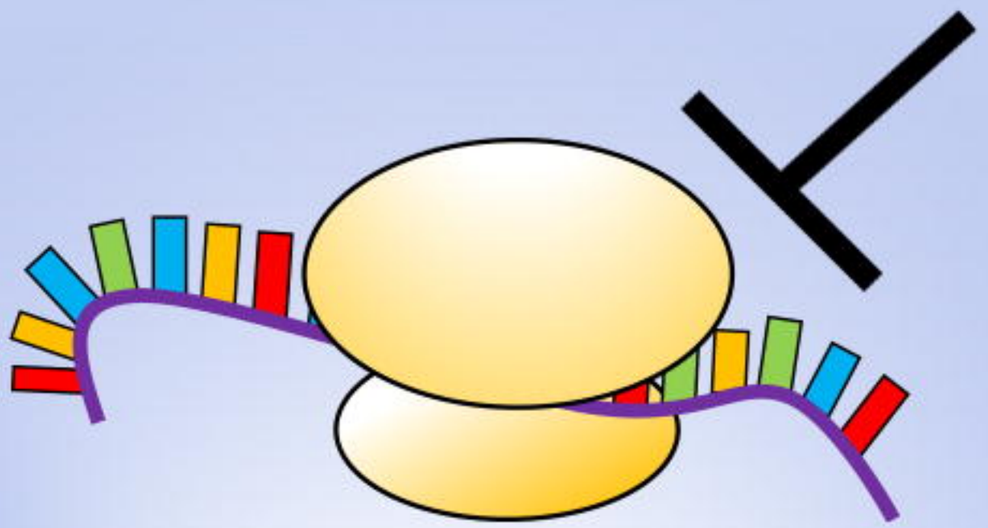

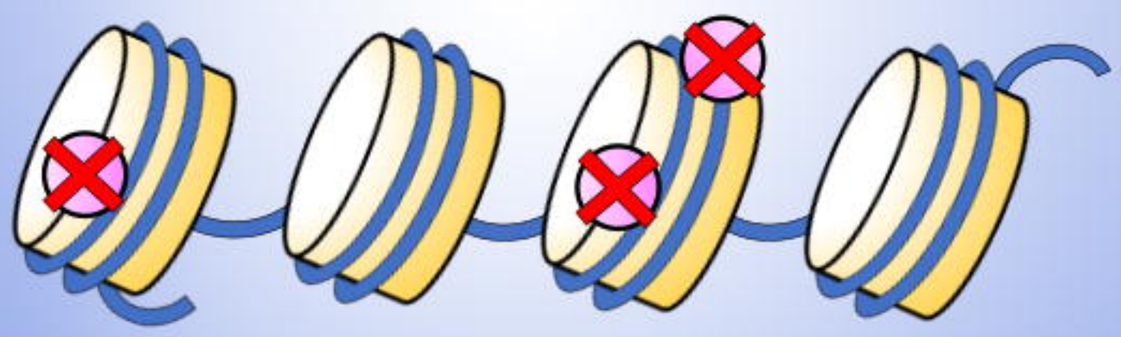

Figure 1.

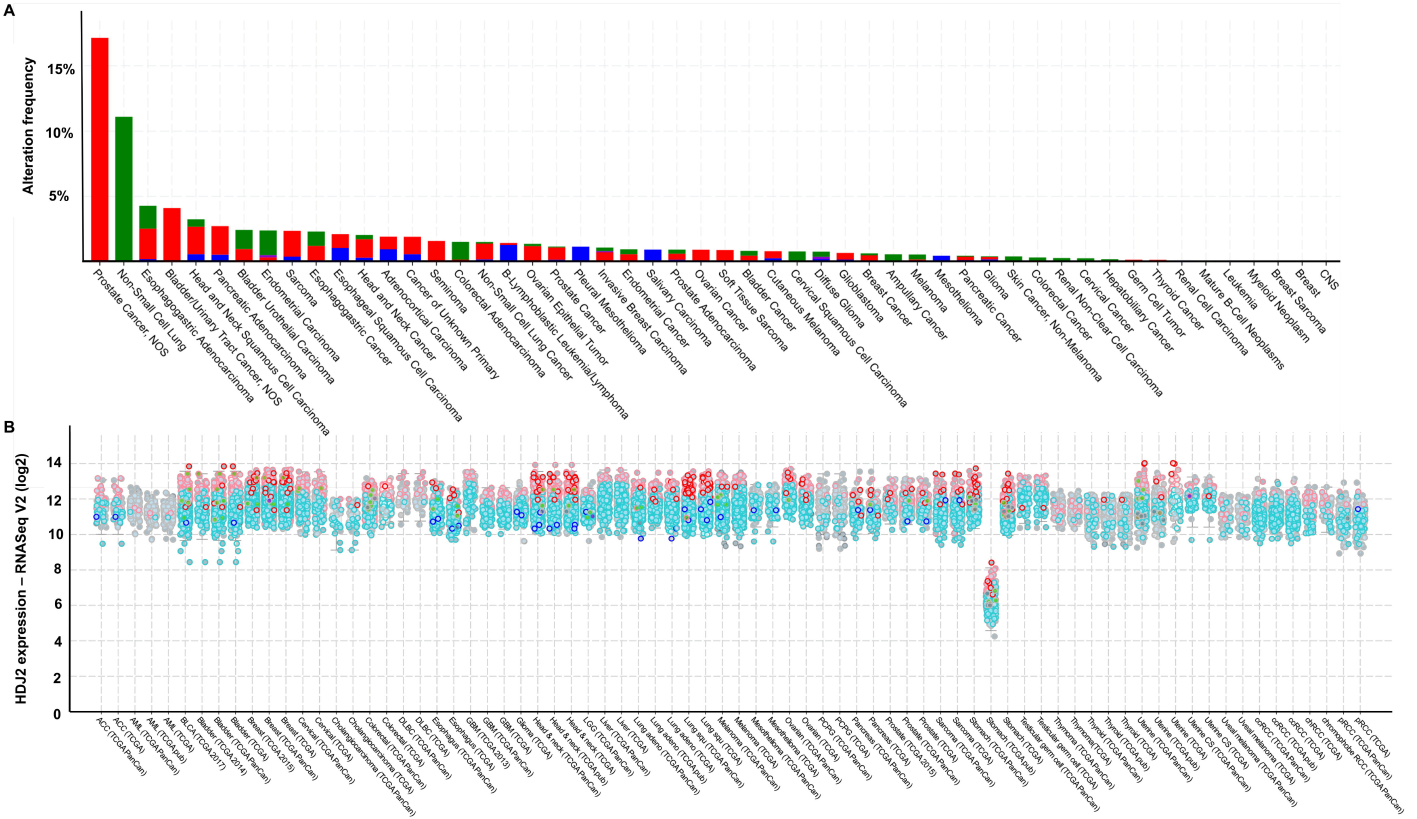
A
Alteration frequency
15%
10%
5%
Prostate Cancer, NOS
Non-Small Cell Lung
Esophagogastric Adenocarcinoma
Bladder/Urinary Tract Cancer, NOS
Head and Neck Squamous Cell Carcinoma
Pancreatic Adenocarcinoma
Bladder Urothelial Carcinoma
Endometrial Carcinoma
Sarcoma
Esophagogastric Cancer
Esophageal Squamous Cell Carcinoma
Head and Neck Cancer
Adrenocortical Carcinoma
Cancer of Unknown Primary
Seminoma
Colorectal Adenocarcinoma
Non-Small Cell Lung Cancer
B-Lymphoblastic Leukemia/Lymphoma
Ovarian Epithelial Tumor
Prostate Cancer
Pleural Mesothelioma
Invasive Breast Carcinoma
Endometrial Cancer
Salivary Carcinoma
Prostate Adenocarcinoma
Ovarian Cancer
Soft Tissue Sarcoma
Bladder Cancer
Cutaneous Melanoma
Cervical Squamous Cell Carcinoma
Diffuse Glioma
Glioblastoma
Breast Cancer
Ampullary Cancer
Melanoma
Mesothelioma
Pancreatic Cancer
Glioma
Skin Cancer, Non-Melanoma
Colorectal Cancer
Renal Non-Clear Cell Carcinoma
Cervical Cancer
Hepatobiliary Cancer
Germ Cell Tumor
Thyroid Cancer
Renal Cell Carcinoma
Mature B-Cell Neoplasms
Leukemia
Myeloid Neoplasm
Breast Sarcoma
Breast
CNS
B
HDJ2 expression – RNASeq V2 (log2)
14
12
10
8
6
4
2
0
ACC (TCGA)
ACC (TCGA,PanCan)
AML (TCGA)
AML (TCGA,Pub)
AML (TCGA,PanCan)
BLCA (TCGA,2017)
Bladder (TCGA,2014)
Bladder (TCGA,PanCan)
Breast (TCGA)
Breast (TCGA,2015)
Breast (TCGA,PanCan)
Cervical (TCGA)
Cervical (TCGA,PanCan)
Cholangiocarcinoma (TCGA)
Cholangiocarcinoma (TCGA,PanCan)
Colorectal (TCGA)
Colorectal (TCGA,PanCan)
DLBC (TCGA)
DLBC (TCGA,PanCan)
Esophagus (TCGA)
Esophagus (TCGA,PanCan)
GBM (TCGA,2013)
GBM (TCGA,PanCan)
Glioma (TCGA)
Head & Neck (TCGA)
Head & Neck (TCGA,PanCan)
LGG (TCGA,PanCan)
Liver (TCGA)
Liver (TCGA,PanCan)
Lung Adeno (TCGA)
Lung Adeno (TCGA,PanCan)
Lung SCC (TCGA)
Lung SCC (TCGA,Pub)
Lung SCC (TCGA,PanCan)
Mesothelioma (TCGA)
Mesothelioma (TCGA,PanCan)
Ovarian (TCGA)
Ovarian (TCGA,PanCan)
PCPG (TCGA)
PCPG (TCGA,PanCan)
Pancreas (TCGA)
Pancreas (TCGA,PanCan)
Prostate (TCGA)
Prostate (TCGA,2015)
Prostate (TCGA,PanCan)
Sarcoma (TCGA)
Sarcoma (TCGA,PanCan)
Stomach (TCGA)
Stomach (TCGA,PanCan)
Testicular germ cell (TCGA,Pub)
Testicular germ cell (TCGA,PanCan)
Thymoma (TCGA)
Thymoma (TCGA,PanCan)
Thyroid (TCGA)
Thyroid (TCGA,Pub)
Uterine (TCGA)
Uterine (TCGA,Pub)
Uterine (TCGA,PanCan)
Uterine CS (TCGA)
Uterine CS (TCGA,PanCan)
Uveal melanoma (TCGA)
Uveal melanoma (TCGA,PanCan)
ccRCC (TCGA)
ccRCC (TCGA,Pub)
ccRCC (TCGA,PanCan)
chRCC (TCGA)
chromophobe RCC (TCGA,PanCan)
pRCC (TCGA)
pRCC (TCGA,PanCan)

Figure 2.

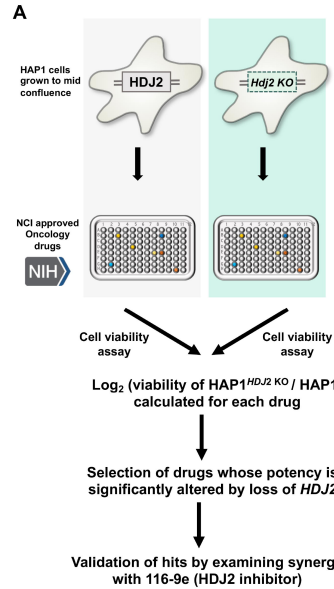
A
HAP1 cells grown to mid confluence
HDJ2
Hdj2 KO
NCI approved Oncology drugs
NIH
Cell viability assay
Cell viability assay
Log2 (viability of HAP1HDJ2 KO / HAP1) calculated for each drug
Selection of drugs whose potency is significantly altered by loss of HDJ2
Validation of hits by examining synergy with 116-9e (HDJ2 inhibitor)

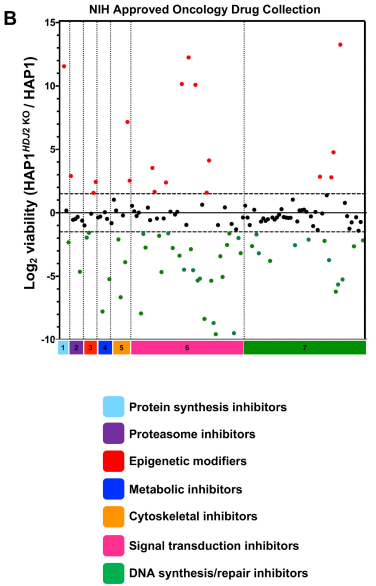
B
NIH Approved Oncology Drug Collection
Log2 viability (HAP1HDJ2 KO / HAP1)
15
10
5
0
-5
-10
1
2
3
4
5
6
7
Protein synthesis inhibitors
Proteasome inhibitors
Epigenetic modifiers
Metabolic inhibitors
Cytoskeletal inhibitors
Signal transduction inhibitors
DNA synthesis/repair inhibitors

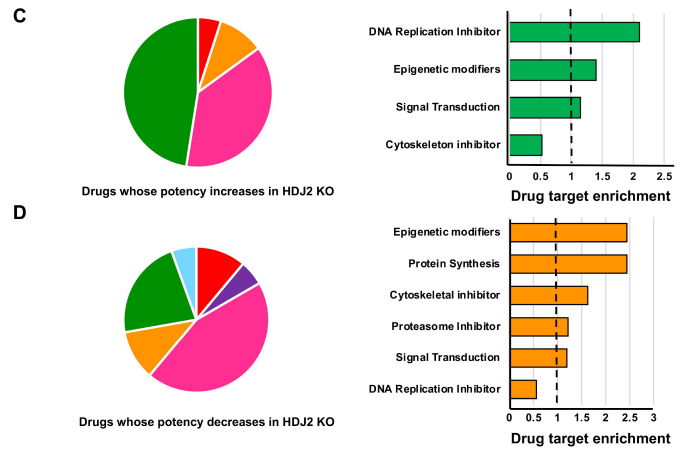
C
Drugs whose potency increases in HDJ2 KO
DNA Replication Inhibitor
Epigenetic modifiers
Signal Transduction
Cytoskeleton inhibitor
0
0.5
1
1.5
2
2.5
Drug target enrichment
D
Drugs whose potency decreases in HDJ2 KO
Epigenetic modifiers
Protein Synthesis
Cytoskeletal inhibitor
Proteasome Inhibitor
Signal Transduction
DNA Replication Inhibitor
0
0.5
1
1.5
2
2.5
3
Drug target enrichment

Figure 3.

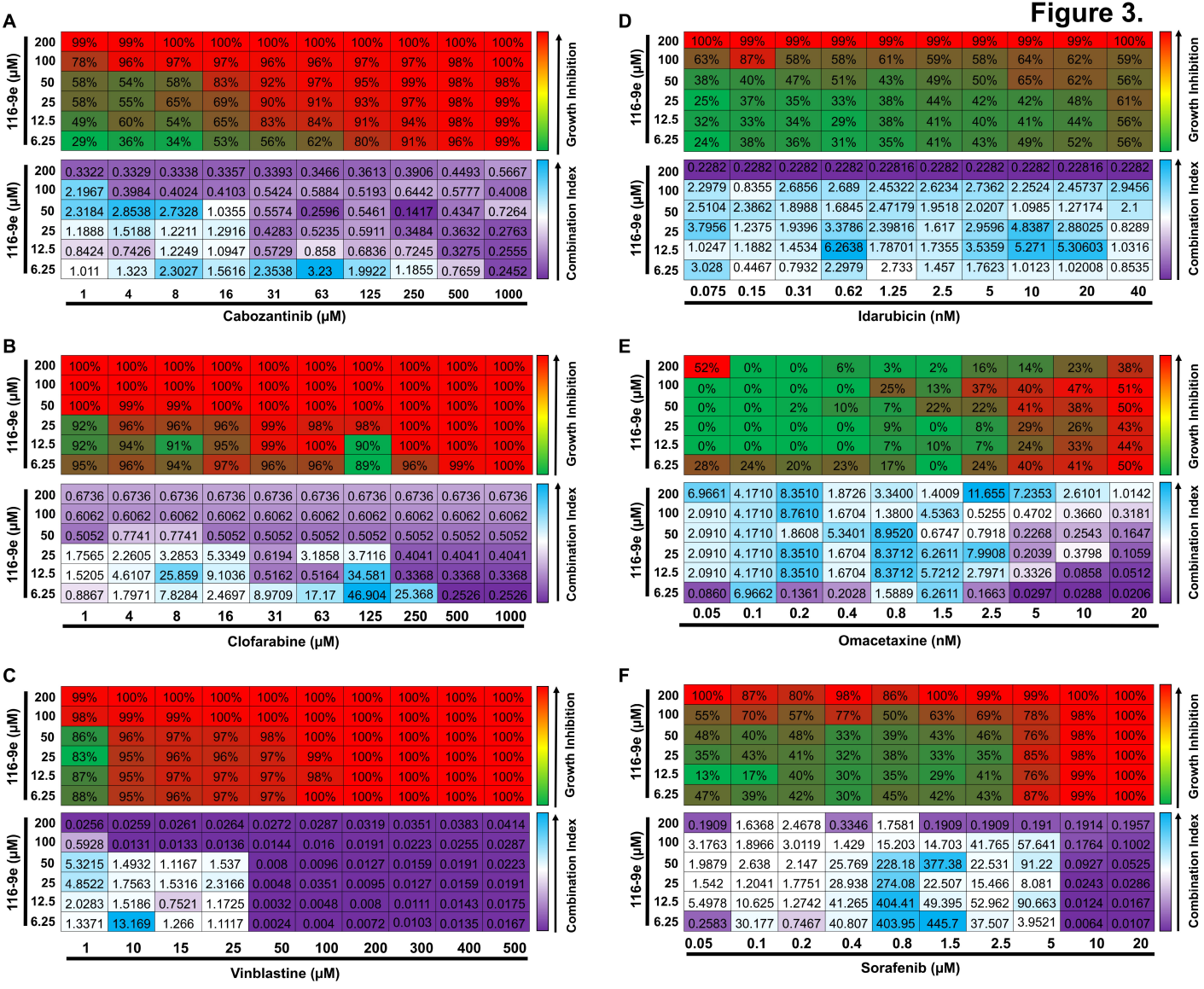
A
116-9e (μM)
200 99% 99% 100% 100% 100% 100% 100% 100% 100% 100%
100 78% 96% 97% 97% 96% 96% 97% 97% 98% 100%
50 58% 54% 58% 83% 92% 97% 95% 99% 98% 98%
25 58% 55% 65% 69% 90% 91% 93% 97% 98% 99%
12.5 49% 60% 54% 65% 83% 84% 91% 94% 98% 99%
6.25 29% 36% 34% 53% 56% 62% 80% 91% 96% 99%
Growth Inhibition
116-9e (μM)
200 0.3322 0.3329 0.3338 0.3357 0.3393 0.3466 0.3613 0.3906 0.4493 0.5667
100 2.1967 0.3984 0.4024 0.4103 0.5424 0.5884 0.5193 0.6442 0.5777 0.4008
50 2.3184 2.8538 2.7328 1.0355 0.5574 0.2596 0.5461 0.1417 0.4347 0.7264
25 1.1888 1.5188 1.2211 1.2916 0.4283 0.5235 0.5911 0.3484 0.3632 0.2763
12.5 0.8424 0.7426 1.2249 1.0947 0.5729 0.858 0.6836 0.7245 0.3275 0.2555
6.25 1.011 1.323 2.3027 1.5616 2.3538 3.23 1.9922 1.1855 0.7659 0.2452
Combination Index
1 4 8 16 31 63 125 250 500 1000
Cabozantinib (μM)
B
116-9e (μM)
200 100% 100% 100% 100% 100% 100% 100% 100% 100% 100%
100 100% 100% 100% 100% 100% 100% 100% 100% 100% 100%
50 100% 99% 99% 100% 100% 100% 100% 100% 100% 100%
25 92% 96% 96% 96% 99% 98% 98% 100% 100% 100%
12.5 92% 94% 91% 95% 99% 100% 90% 100% 100% 100%
6.25 95% 96% 94% 97% 96% 96% 89% 96% 99% 100%
Growth Inhibition
116-9e (μM)
200 0.6736 0.6736 0.6736 0.6736 0.6736 0.6736 0.6736 0.6736 0.6736 0.6736
100 0.6062 0.6062 0.6062 0.6062 0.6062 0.6062 0.6062 0.6062 0.6062 0.6062
50 0.5052 0.7741 0.7741 0.5052 0.5052 0.5052 0.5052 0.5052 0.5052 0.5052
25 1.7565 2.2605 3.2853 5.3349 0.6194 3.1858 3.7116 0.4041 0.4041 0.4041
12.5 1.5205 4.6107 25.859 9.1036 0.5162 0.5164 34.581 0.3368 0.3368 0.3368
6.25 0.8867 1.7971 7.8284 2.4697 8.9709 17.17 46.904 25.368 0.2526 0.2526
Combination Index
1 4 8 16 31 63 125 250 500 1000
Clofarabine (μM)
C
116-9e (μM)
200 99% 100% 100% 100% 100% 100% 100% 100% 100% 100%
100 98% 99% 99% 100% 100% 100% 100% 100% 100% 100%
50 86% 96% 97% 97% 98% 100% 100% 100% 100% 100%
25 83% 95% 96% 96% 97% 99% 100% 100% 100% 100%
12.5 87% 95% 97% 97% 97% 98% 100% 100% 100% 100%
6.25 88% 95% 96% 97% 97% 100% 100% 100% 100% 100%
Growth Inhibition
116-9e (μM)
200 0.0256 0.0259 0.0261 0.0264 0.0272 0.0287 0.0319 0.0351 0.0383 0.0414
100 0.5928 0.0131 0.0133 0.0136 0.0144 0.016 0.0191 0.0223 0.0255 0.0287
50 5.3215 1.4932 1.1167 1.537 0.008 0.0096 0.0127 0.0159 0.0191 0.0223
25 4.8522 1.7563 1.5316 2.3166 0.0048 0.0351 0.0095 0.0127 0.0159 0.0191
12.5 2.0283 1.5186 0.7521 1.1725 0.0032 0.0048 0.008 0.0111 0.0143 0.0175
6.25 1.3371 13.169 1.266 1.1117 0.0024 0.004 0.0072 0.0103 0.0135 0.0167
Combination Index
1 10 15 25 50 100 200 300 400 500
Vinblastine (μM)
D
116-9e (μM)
200 100% 99% 99% 99% 99% 99% 99% 99% 99% 100%
100 63% 87% 58% 58% 61% 59% 58% 64% 62% 59%
50 38% 40% 47% 51% 43% 49% 50% 65% 62% 56%
25 25% 37% 35% 33% 38% 44% 42% 42% 48% 61%
12.5 32% 33% 34% 29% 38% 41% 40% 41% 44% 56%
6.25 24% 38% 36% 31% 35% 41% 43% 49% 52% 56%
Growth Inhibition
116-9e (μM)
200 0.2282 0.2282 0.2282 0.2282 0.22816 0.2282 0.2282 0.2282 0.22816 0.2282
100 2.2979 0.8355 2.6856 2.689 2.45322 2.6234 2.7362 2.2524 2.45737 2.9456
50 2.5104 2.3862 1.8988 1.6845 2.47179 1.9518 2.0207 1.0985 1.27174 2.1
25 3.7956 1.2375 1.9396 3.3786 2.39816 1.617 2.9596 4.8387 2.88025 0.8289
12.5 1.0247 1.1882 1.4534 6.2638 1.78701 1.7355 3.5359 5.271 5.30603 1.0316
6.25 3.028 0.4467 0.7932 2.2979 2.733 1.457 1.7623 1.0123 1.02008 0.8535
Combination Index
0.075 0.15 0.31 0.62 1.25 2.5 5 10 20 40
Idarubicin (nM)
E
116-9e (μM)
200 52% 0% 0% 6% 3% 2% 16% 14% 23% 38%
100 0% 0% 0% 0% 25% 13% 37% 40% 47% 51%
50 0% 0% 2% 10% 7% 22% 22% 41% 38% 50%
25 0% 0% 0% 0% 9% 0% 8% 29% 26% 43%
12.5 0% 0% 0% 0% 7% 10% 7% 24% 33% 44%
6.25 28% 24% 20% 23% 17% 0% 24% 40% 41% 50%
Growth Inhibition
116-9e (μM)
200 6.9661 4.1710 8.3510 1.8726 3.3400 1.4009 11.655 7.2353 2.6101 1.0142
100 2.0910 4.1710 8.7610 1.6704 1.3800 4.5363 0.5255 0.4702 0.3660 0.3181
50 2.0910 4.1710 1.8608 5.3401 8.9520 0.6747 0.7918 0.2268 0.2543 0.1647
25 2.0910 4.1710 8.3510 1.6704 8.3712 6.2611 7.9908 0.2039 0.3798 0.1059
12.5 2.0910 4.1710 8.3510 1.6704 8.3712 5.7212 2.7971 0.3326 0.0858 0.0512
6.25 0.0860 6.9662 0.1361 0.2028 1.5889 6.2611 0.1663 0.0297 0.0288 0.0206
Combination Index
0.05 0.1 0.2 0.4 0.8 1.5 2.5 5 10 20
Omacetaxine (nM)
F
116-9e (μM)
200 100% 87% 80% 98% 86% 100% 99% 99% 100% 100%
100 55% 70% 57% 77% 50% 63% 69% 78% 98% 100%
50 48% 40% 48% 33% 39% 43% 46% 76% 98% 100%
25 35% 43% 41% 32% 38% 33% 35% 85% 98% 100%
12.5 13% 17% 40% 30% 35% 29% 41% 76% 99% 100%
6.25 47% 39% 42% 30% 45% 42% 43% 87% 99% 100%
Growth Inhibition
116-9e (μM)
200 0.1909 1.6368 2.4678 0.3346 1.7581 0.1909 0.1909 0.191 0.1914 0.1957
100 3.1763 1.8966 3.0119 1.429 15.203 14.703 41.765 57.641 0.1764 0.1002
50 1.9879 2.638 2.147 25.769 228.18 377.38 22.531 91.22 0.0927 0.0525
25 1.542 1.2041 1.7751 28.938 274.08 22.507 15.466 8.081 0.0243 0.0286
12.5 5.4978 10.625 1.2742 41.265 404.41 49.395 52.962 90.663 0.0124 0.0167
6.25 0.2583 30.177 0.7467 40.807 403.95 445.7 37.507 3.9521 0.0064 0.0107
Combination Index
0.05 0.1 0.2 0.4 0.8 1.5 2.5 5 10 20
Sorafenib (μM)

Figure 4.

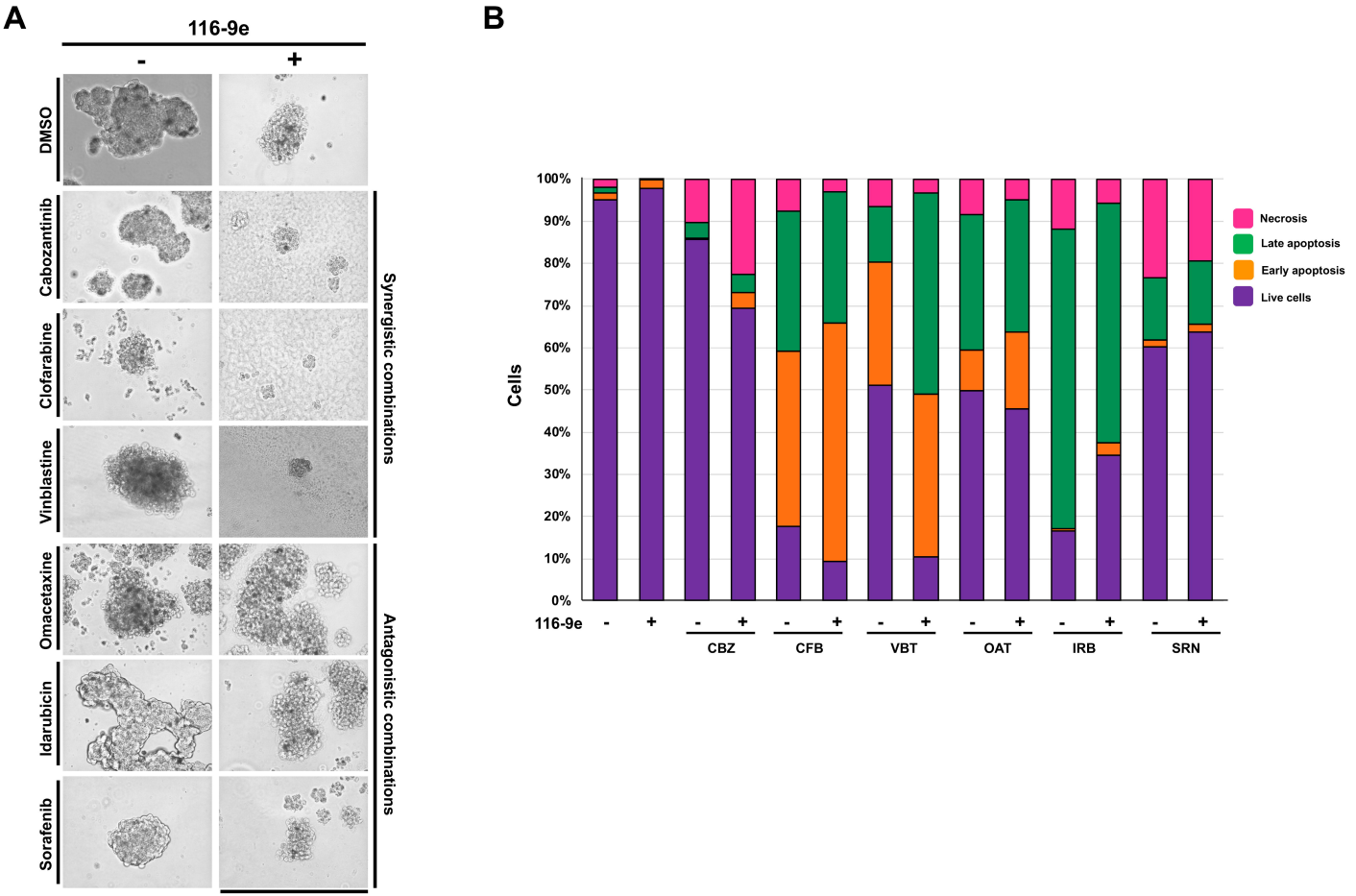
A
116-9e
-
+
DMSO
Cabozantinib
Clofarabine
Vinblastine
Omacetaxine
Idarubicin
Sorafenib
Synergistic combinations
Antagonistic combinations
100 μM
B
Cells
100%
90%
80%
70%
60%
50%
40%
30%
20%
10%
0%
116-9e
CBZ
CFB
VBT
OAT
IRB
SRN
Necrosis
Late apoptosis
Early apoptosis
Live cells